JGS
Journal of the Geological Society

Research article

Published online November 21, 2017

https://doi.org/10.1144/jgs2017-036 | Vol. 175 | 2018 | pp. 247–262

Sedimentology and microfacies of a mud-rich slope succession: in the Carboniferous Bowland Basin, NW England (UK)

Sarah M. Newport[1]*, Rhodri M. Jerrett[1], Kevin G. Taylor[1], Edward Hough[2] & Richard H. Worden[3]

[1] School of Earth, Atmospheric, and Environmental Sciences, University of Manchester, Manchester M13 9PL, UK
[2] British Geological Survey, Environmental Science Centre, Nicker Hill, Keyworth, Nottingham NG12 5GG, UK
[3] School of Environmental Sciences, University of Liverpool, Jane Herdman Building, Liverpool L69 3GP, UK
* Correspondence: sarah.m.newport@manchester.ac.uk

Abstract: A paucity of studies on mud-rich basin slope successions has resulted in a significant gap in our sedimentological understanding in these settings. Here, macro- and micro-scale analysis of mudstone composition, texture and organic matter was undertaken on a continuous core through a mud-dominated slope succession from the Marl Hill area in the Carboniferous Bowland Basin. Six lithofacies, all dominated by turbidites and debrites, combine into three basin slope facies associations: sediment-starved slope, slope dominated by low-density turbidites and slope dominated by debrites. Variation in slope sedimentation was a function of relative sea-level change, with the sediment-starved slope occurring during maximum flooding of the contemporaneous shelf, and the transition towards a slope dominated by turbidites and then debrites occurring during normal or forced shoreline progradation towards the shelf margin. The sediment-starved slope succession is dominated by Type II kerogen, whereas the slope dominated by low-density turbidites is dominated by Type III kerogen. This study suggests that mud-dominated lower slope settings are largely active depositional sites, with consistent evidence for sediment traction. Additionally, the composition and texture of basin slope mudstones, as well as organic content, vary predictably as a function of shelf processes linked to relative sea-level change.

Received 10 March 2017; **revised** 6 September 2017; **accepted** 11 September 2017

The recent development of unconventional hydrocarbon systems that target source rock reservoirs (organic-rich mudstones acting as both source and reservoir) has led to a re-evaluation of fundamental geological processes operating in fine-grained sedimentary systems (e.g. Ross & Bustin 2009; Aplin & Macquaker 2011; Jarvie 2012; Hart *et al.* 2013; Taylor & Macquaker 2014). Depositional and post-depositional processes within fine-grained sedimentary systems are complex and control the distribution of rock properties, both spatially and temporally, which are key considerations for the appraisal, exploration and production of source rock reservoirs (e.g. Jarvie *et al.* 2007; Loucks *et al.* 2009, 2012; Charpentier & Cook 2011; Andrews 2013). The style of deposition (e.g. the amount of organic matter flux, the type of organic matter present, the detrital grain assemblage, the sediment accumulation rate) is therefore critical in determining the characteristics and variability within any fine-grained sedimentary succession (e.g. Macquaker *et al.* 2007; Milliken *et al.* 2012; Hart *et al.* 2013; Milliken 2014; Lazar *et al.* 2015*a*; Schieber 2016*a*). Previous work on mud depositional settings has principally focused on processes acting on shelf (e.g. Schieber 2007; Macquaker *et al.* 2010; Schieber *et al.* 2010; Davies *et al.* 2012; Bohacs *et al.* 2014) or basin floor successions (e.g. Könitzer *et al.* 2014; Schieber 2016*b*). By focusing on the sedimentology and the resulting mudstone textures and variability, this paper aims to address the knowledge gap of processes acting on mud-dominated slope successions. The specific questions addressed in this study are as follows.

(1) What are the dominant modes of deposition active within a mud-rich slope succession?
(2) Is slope sedimentation inherently linked to contemporaneous shelf sedimentation?
(3) Is there a discernible relationship between the type and content of the organic matter of facies and facies associations within a slope succession?

These detailed sedimentological observations have been made on a continuous core (Marl Hill: MHD11; British Geological Survey reference number SD64NE/20), that preserves the transition from carbonate-dominated to clastic-dominated mudstone deposition, within a marginal to basinal mudstone succession, from an active exploration play, the Bowland Shale Formation (Carboniferous, UK).

Geological setting of the Bowland Basin

During the Viséan and Namurian stages of the Carboniferous (347 – 318 Ma; Figs 1 and 2), a series of interconnected half-graben basins within the Pennine Province (northern England, UK) formed part of a shallow epicontinental seaway that stretched across the Laurussian continent, with long-lived palaeogeographical barriers to the north (Southern Uplands High) and to the south (Wales–London–Brabant High; Woodcock & Strachan 2002; Davies 2008; Waters *et al.* 2009).

The interconnected half-grabens of the Pennine Province formed as a result of back-arc rift extension related to the Variscan Orogeny (410 – 280 Ma), with a strong NW–SE and NE–SW orientation inherited from pre-existing Caledonian structures (Fraser & Gawthorpe 1990). The Bowland Basin, the focus of this study, is a complex NE–SW-trending fault-controlled half-graben within the larger Craven Basin (Fig. 1). The margins of the Bowland Basin are defined by the Bowland Line to the north, the Craven Fault System to the NE (forming the boundary with the Askrigg Block 'high'), and the Pendle Fault to the south (forming the boundary with the Central Lancashire High; Gawthorpe 1987; Arthurton *et al.* 1988; Riley 1990; Fraser & Gawthorpe 2003). Initiation of the Bowland Basin occurred in the latest Devonian to Tournaisian, with two further distinct episodes of rifting occurring during the Chadian–Arundian and Asbian–Brigantian (Gawthorpe 1987). Within the

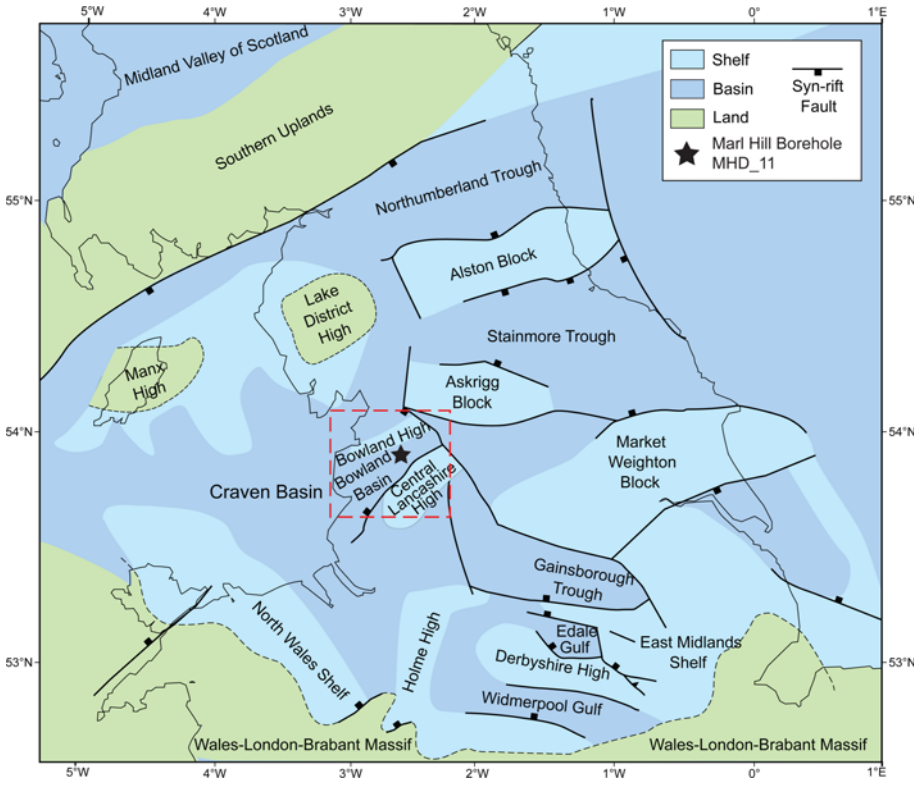

Fig. 1. Palaeogeographical map of northern England (UK) during the Carboniferous with modern geographical outline of the UK shown (adapted from Waters *et al.* 2009). The red box indicates the area of this study, the Bowland Basin (also known as the Craven Basin).

Bowland Basin a number of lesser depositional highs are present, which were primarily controlled by SW–NE-trending reactivated Caledonian basement faults (Gawthorpe 1987; Riley 1990; Waters *et al.* 2009). Depositional environments in the Bowland Basin evolved from a carbonate ramp to carbonate-rimmed shelf, with a distinct shelf–slope–basin-floor morphology through the Tournaisian to Visean (Gawthorpe 1987). Clastic deep-water sedimentation began to replace carbonate sedimentation from the late Visean onwards (Aitkenhead *et al.* 1992; Brandon *et al.* 1998; Kirby *et al.* 2000; Kane 2010), with progradation of the Millstone Grit deltas into the study area from the north during the late Pendleian. The Bowland Shale Formation typically has a thickness of 120 – 620 m (Waters *et al.* 2009), thickening southwestward towards the Pendle Fault (Evans & Kirby 1999). Within the Bowland Basin the deposition of thick mud-rich successions has been interpreted as the result of hemipelagic settling from suspension, largely below the storm wave-base, interrupted by periodic input from carbonate-rich and siliciclastic-rich turbidites and possibly storm events (e.g. Aitkenhead *et al.* 1992; Waters *et al.* 2009).

Stratigraphy of Marl Hill borehole MHD11

The Marl Hill borehole MHD11 core [SD 6833 4683] was collected by BP Mineral International Ltd for the purpose of prospecting for Pb–Zn mineralization associated with the proximal Clitheroe Fault Zone. The core is currently stored by the British Geological Survey at Keyworth (UK). The core penetrates a 300.58 m succession consisting of the following stratigraphic intervals: Worston Shale Group (consisting of the Hodder Mudstone Formation, Limekiln Wood Limestone Formation and Hodderense Limestone Formation) and Bowland Shale Group (consisting of the Pendleside Limestone Formation, Lower Bowland Shale Formation and Upper Bowland Shale Formation; Fig. 2; Aitkenhead *et al.* 1992). Based on a revised stratigraphic framework for the Carboniferous rocks of Britain (Waters *et al.* 2009, 2011), this interval equates to the Craven Group, consisting of the Hodder Mudstone Formation, Hodderense Limestone Formation, Pendleside Limestone Formation and Bowland Shale Formation. It is useful to refer to the former stratigraphic nomenclature as this allows correlation with older, established stratigraphies such as the seismic stratigraphy of Fraser & Gawthorpe (2003).Three marine bands are present within the cored Bowland Shale interval, the B_{2b} *Goniatites globostriatus* (*Beyrichoceras* biozone, Upper Asbian), P_2 *Sudeticeras* (Upper Brigantian) and E_{1a} *Emstites (Cravenoceras) leion* (Lower Pendleian) (Figs 2 and 3; Riley 1988; Aitkenhead *et al.* 1992). The focus of this study is the succession from 5 to 125 m consisting of the Hodder Mudstone Formation, Hodderense Limestone Formation, Pendleside Limestone Formation and Bowland Shale Formation. The core is slabbed, and recovery of the core in the interval from 5 to 125 m is *c.* 95%.

Methods

The illuminated, wetted core was logged for macroscopically visible textural (grain-size) and compositional changes, sedimentary features and fossil content at 10 cm resolution. The mudstone was classified according to the scheme of Lazar *et al.* (2015*b*). That is, sediments consisting of greater than two-thirds of grains <8 μm are defined as claystones, those with grains of 8 to < 32 μm are defined as mudstones and those containing two-thirds of grains of 32 to < 62.5 μm are defined as siltstones. The compositional modifier 'argillaceous', 'calcareous' or 'siliceous' is added where >50% of the material comprises clay, carbonate or quartz, respectively. Compositional proportions for all scales (e.g. at core, scanned, optical microscope and SEM scale) were assessed using visual estimates. The core was subdivided into lithofacies according to these macroscale observations, and 36 samples were collected to prepare thin sections for identification of micro-scale features within these facies.

A total of 82 samples were taken across the cored interval, with 75 from the Bowland Shale Formation, using an adjusted uniform sampling method of one sample per metre of core with additional samples taken at points of interest. A further six spot samples were taken from the underlying Pendleside Limestone and Hodder

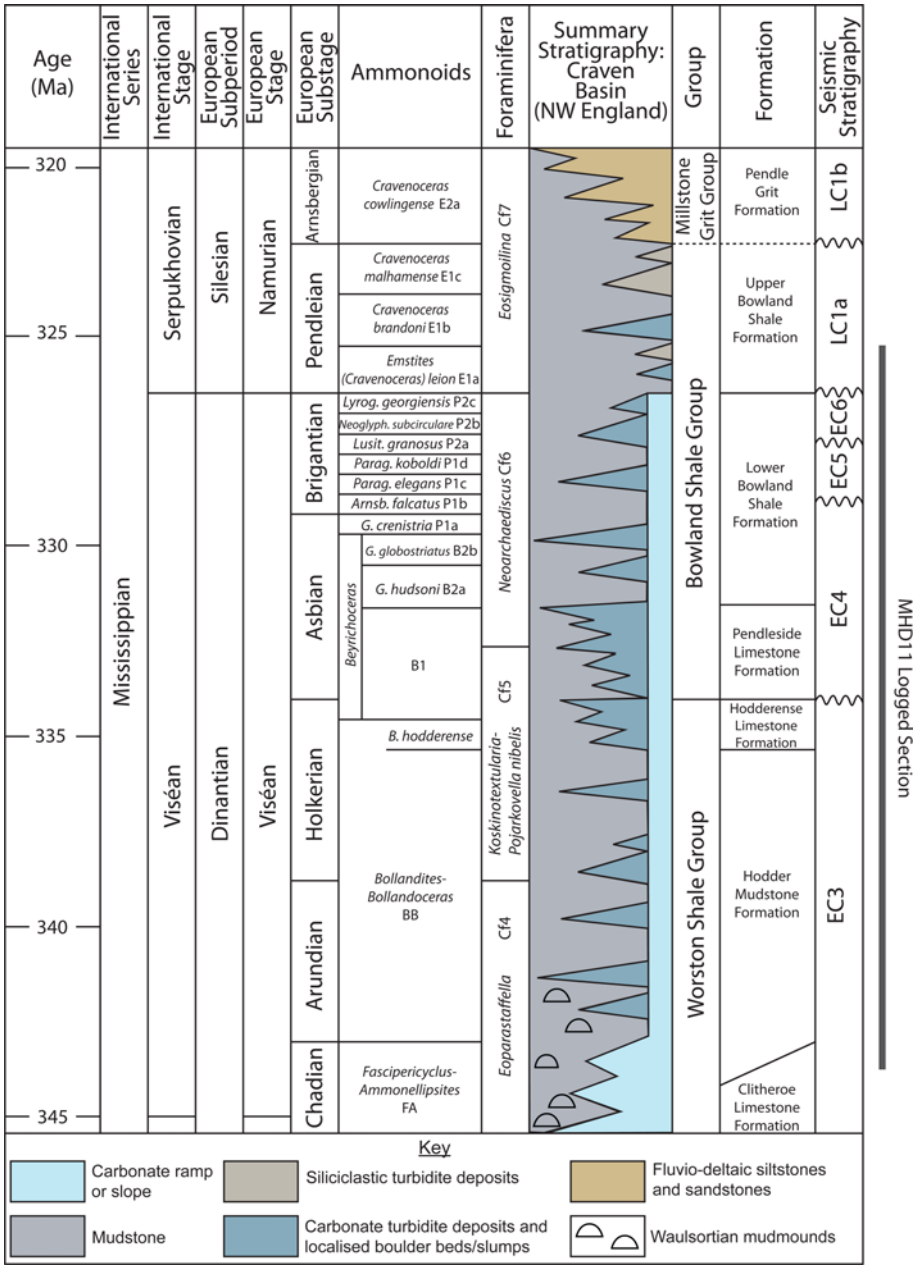

Fig. 2. Summary of the lithostratigraphy of the Craven Basin (modified from Waters *et al.* 2009), showing ammonoid zones (after Riley 1993; Waters & Condon 2012), foraminifera zones (after Riley 1993; Somerville 2008), lithostratigraphy (after Gawthorpe 1986; Riley 1990; Aitkenhead *et al.* 1992) and seismic stratigraphy (after Fraser & Gawthorpe 2003).

Mudstone Formations (Figs 2 and 3). A total of 36 thin sections were chosen to represent all mudstone macrofacies identified at core scale, and prepared for polished (uncovered) thin sections normal to principal bedding orientation (Figs 3 and 4). All thin sections were scanned using an EPSON Perfection V600 Photo at 2400 d.p.i. resolution. Optical microscopy was undertaken using a Nikon Eclipse LV100NPOL microscope fitted with a Nikon DS-Fi2 camera. Scanning electron microscopy with an FEI XL30 Environmental scanning electron microscope with a backscattered electron detector attached was used for high-resolution imaging and compositional analysis.

Total organic carbon (TOC) was measured from 50 spot samples using a Leco CS230 carbon analyser, before analysis sample aliquots were de-calcified using 5M HCl and rinsed five times. Iron chip (0.7 g) and 'Lecocell' (tungsten) accelerants (*c.* 1.5 g) were then added to the crucibles. An induction furnace heated the samples to *c.* 1500°C in an oxygen atmosphere and the resulting CO_2 was quantified using an IR detector. The instrument was calibrated using Leco supplied certified carbon standards appropriate to the carbon content of the samples being analysed; replicate and blank analyses were also carried out.

RockEval™ analysis was undertaken using a RockEval™ VI analyser. RockEval™ is a pyrolysis-based technique and results can be interpreted to indicate the type and maturity of organic matter and thus its petroleum generation potential (Espitalié *et al.* 1977). Between 50 and 100 mg of powdered whole-rock samples were pyrolysed in an inert helium atmosphere from 180 to 600°C, using a ramp rate of 25°C min^{-1}. The mass of hydrocarbon vapours produced at 300°C (free hydrocarbons) was analysed using a flame ionizing detector (FID; S_1 peak of the pyrogram). The temperature was then increased from 300 to 550°C to crack non-volatile organic matter (i.e. kerogen) (producing the S_2 peak of the pyrogram, CO_2 and water). The temperature at which the S_2 peak reaches maximum generation is termed the T_{max} and is a proxy for thermal maturity. The CO_2 generated during thermal breakdown of kerogen is recorded as the S_3 peak of the pyrogram. Further parameters were derived using the following equations (Tissot & Welte 1984): (1) hydrogen index, $HI = (S_2/TOC) \times 100$; (2) oxygen index, $OI = (S_3/TOC) \times 100$; (3) production index, $PI = S_1/(S_1 + S_2)$; (4) transformation index, $TI = S_1/TOC$; (5) pyrolysate yield, $PY = S_1 + S_2$. All organic matter values either measured (using TOC or RockEval methods) or calculated reported in this study are present-day values.

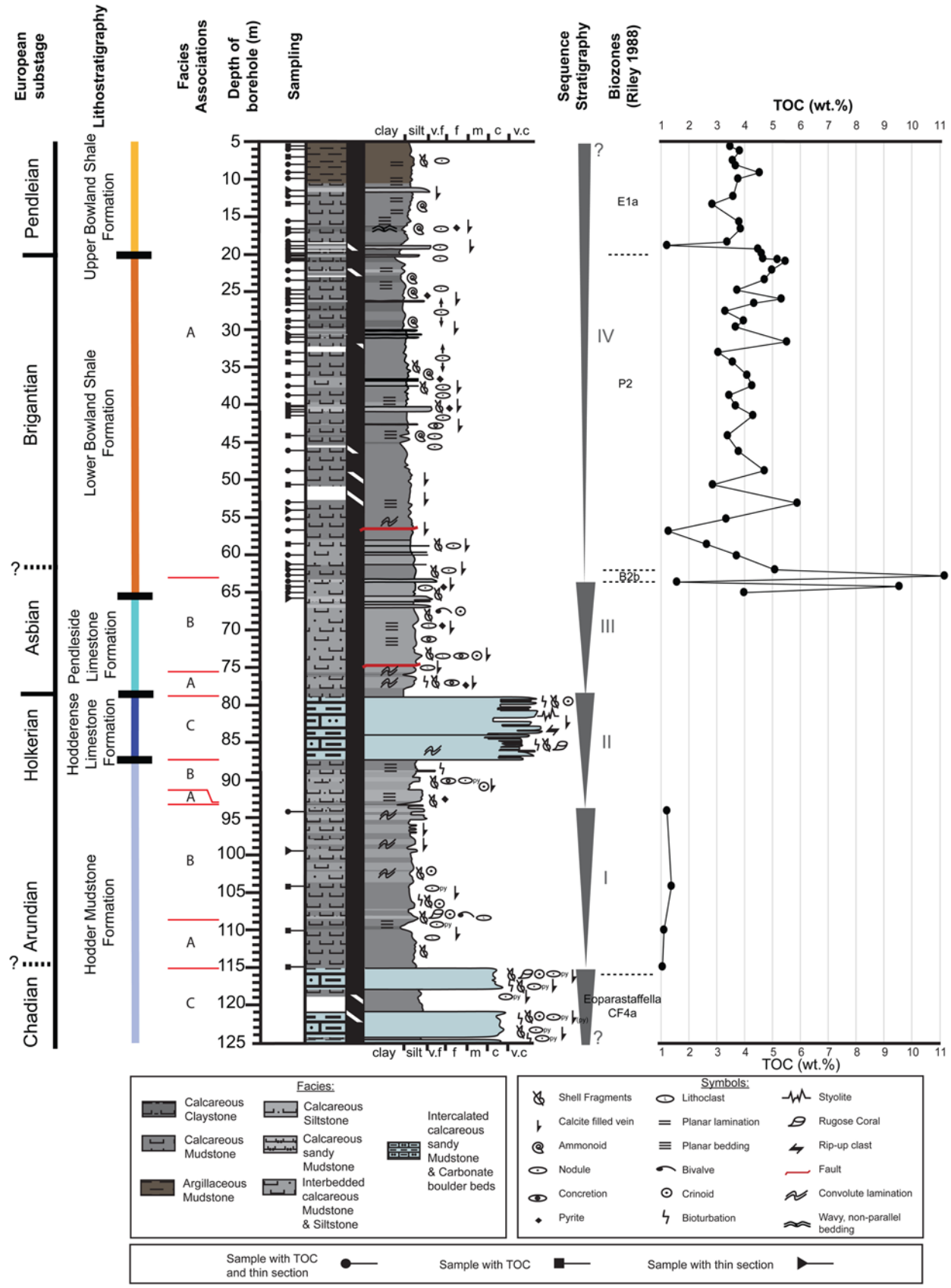

Fig. 3. Sedimentary log of Marl Hill (MHD11) core material, including microfacies features, sample locations, TOC and biozones (after Riley 1988). Diagonal white lines in dark bar indicate core in a fragmentary state.

Lithofacies analysis

The mud-rich succession in the Marl Hill core contains a total of six lithofacies comprising calcareous claystone, calcareous mudstone, argillaceous mudstone, calcareous siltstone, calcareous sandy mudstone and matrix-supported carbonate conglomerate (Facies 1–6 respectively; Figs 3 and 4). The mudstone lithofacies were

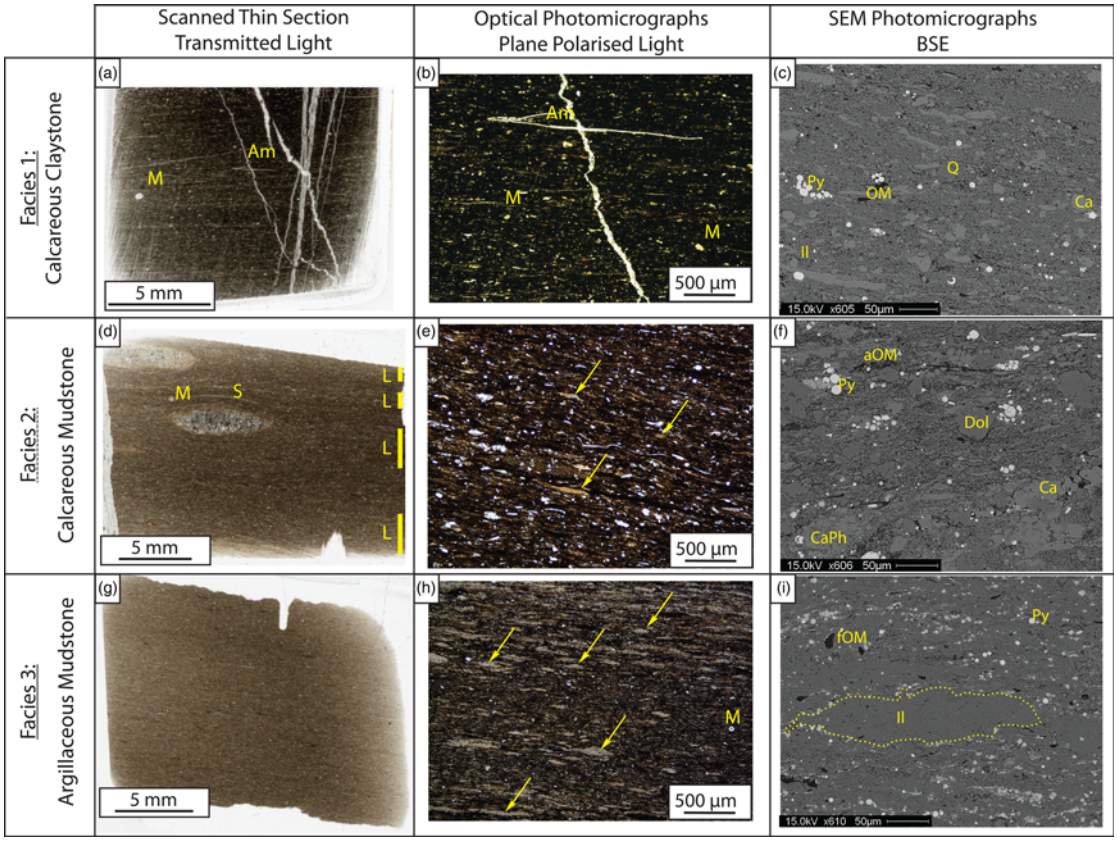

Fig. 4. Summary table of the six microfacies identified within the Marl Hill borehole (MHD11). Facies 1: calcareous claystone. (**a**) Scanned: MHD11_52 (41 m, Brigantian); fine mudstone, calcareous, continuous planar parallel laminasets, varying in colour (dark, more clay rich; light, also containing larger numbers of fossils and lenticular fabric). One large ammonoid shell (Am, <1.5 mm), microfossils (M, possible agglutinated foraminifera, <400 µm). Calcite veins show at least two phases. (**b**) Optical: MHD11_52 (41 m, Brigantian); close-up of ammonoid fossil fragment with crosscutting calcite vein, numerous recrystallized carbonate fragments and minor compacted shale intraclasts present (<250 µm). (**c**) SEM: MHD11_39 (30.6 m, Brigantian) BSE SEM image; fine mudstone (claystone), with calcite grains (biogenic and detrital with minor authigenic, <40 µm), minor quartz (Q), pyrite (Py), illitic clay matrix and organic matter (OM). Facies 2: calcareous mudstone. (**d**) Scanned: MHD11_17 (18.3 m, Pendleian); medium mudstone, calcareous with coarse calcite grains (<60 µm, detrital and biogenic), undetermined shell fragments (S), discontinuous, wavy parallel laminations. Laminasets show colour variations (light highlighted, L) associated with variations in clay. Compacted composite grains (intraclasts and possible organo-mineralic aggregates) form lenses (<500 µm). Differential compaction around nodules (calcite rimmed with calcium phosphate and dolomite). Pyrite dispersed and localized with nodules. (**e**) Optical: MHD11_17 (18.3 m, Pendleian); lenticular fabric within darker laminasets, recrystallized carbonate grains and compacted composite grains (<400 µm, intraclasts highlighted by arrows). (**f**) SEM: MHD11_26 (20.9 m, Brigantian) BSE SEM image; medium mudstone, calcareous with dispersed carbonate grains (<50 µm; Dol, authigenic dolomite; Ca, calcite), localized calcium phosphate (CaPh), framboidal pyrite, organic matter (predominantly amorphous, aOM) and clay (mainly illitic). Facies 3: argillaceous mudstone. (**g**) Scanned: MHD11_8 (9.9 m, Pendleian); medium mudstone, argillaceous with few coarse calcite grains (<50 µm, biogenic and detrital), homogeneous bed with discontinuous, wavy parallel (inclined) laminations. Compacted composite grains (intraclasts and possible organo-mineralic aggregates) form lenses (<500 µm). (**h**) Optical: MHD11_5 (8.1 m, Pendleian); medium mudstone, argillaceous with few coarse calcite grains (<50 µm) discontinuous, planar parallel laminations. Lenticular fabric of compacted shale intraclasts (<800 µm; highlighted by arrows). Laminasets vary between clay-rich and lens-rich, with microfossils (M, foraminifera, <30 µm) most common in the latter. (**i**) SEM: MHD11_5 (8.1 m, Pendleian) BSE SEM image; medium mudstone, argillaceous with lenticular fabric of compacted soft sediment clasts, surrounded by a pyrite-rich (Py) clay (predominantly illitic clay, Il) matrix with predominantly fragmentary organic matter particles (<25 µm, fOM). Facies 4: calcareous detrital siltstone.

defined according to their macroscopic texture and composition, following the classification scheme of Lazar *et al.* (2015*b*). Images of thin section scans, optical photomicrographs and SEM photomicrographs of each lithofacies are provided in Figure 4. The macroscopic and microscopic sedimentological, biogenic and diagenetic features of each lithofacies are summarized in Table 1. Interpreted depositional processes for each lithofacies are also given in Table 1.

Facies associations

Three facies associations have been identified, and are summarized below. They are here interpreted within the context of a shelf–slope–basin-floor system, previously determined for the study area during the mid-Carboniferous by Gawthorpe (1986, 1987).

Facies Association A: sediment-starved slope

This facies association comprises successions up to 58 m thick (Fig. 3), predominantly composed of calcareous mudstone (Facies 2) and argillaceous mudstone (Facies 3), intercalated with minor calcareous claystone (Facies 1), calcareous siltstone (Facies 4) and calcareous sandy mudstones (Facies 5). Facies 1, 4 and 5 occur as individual thin beds rarely thicker than 20 cm. This facies association represents deposition dominated by low-energy turbidites (predominantly T_3–T_8, with minor T_0–T_2 of Stow & Shanmugam 1980), in which the sediment was originally sourced from areas of carbonate productivity and clastic sediment supply. The presence of mudstone lenses in Facies 1, 2 and 3 suggests that mud-rich sediment was remobilized from a partially lithified substrate, transported via traction and incorporated within the succession. This facies association is the only one to contain

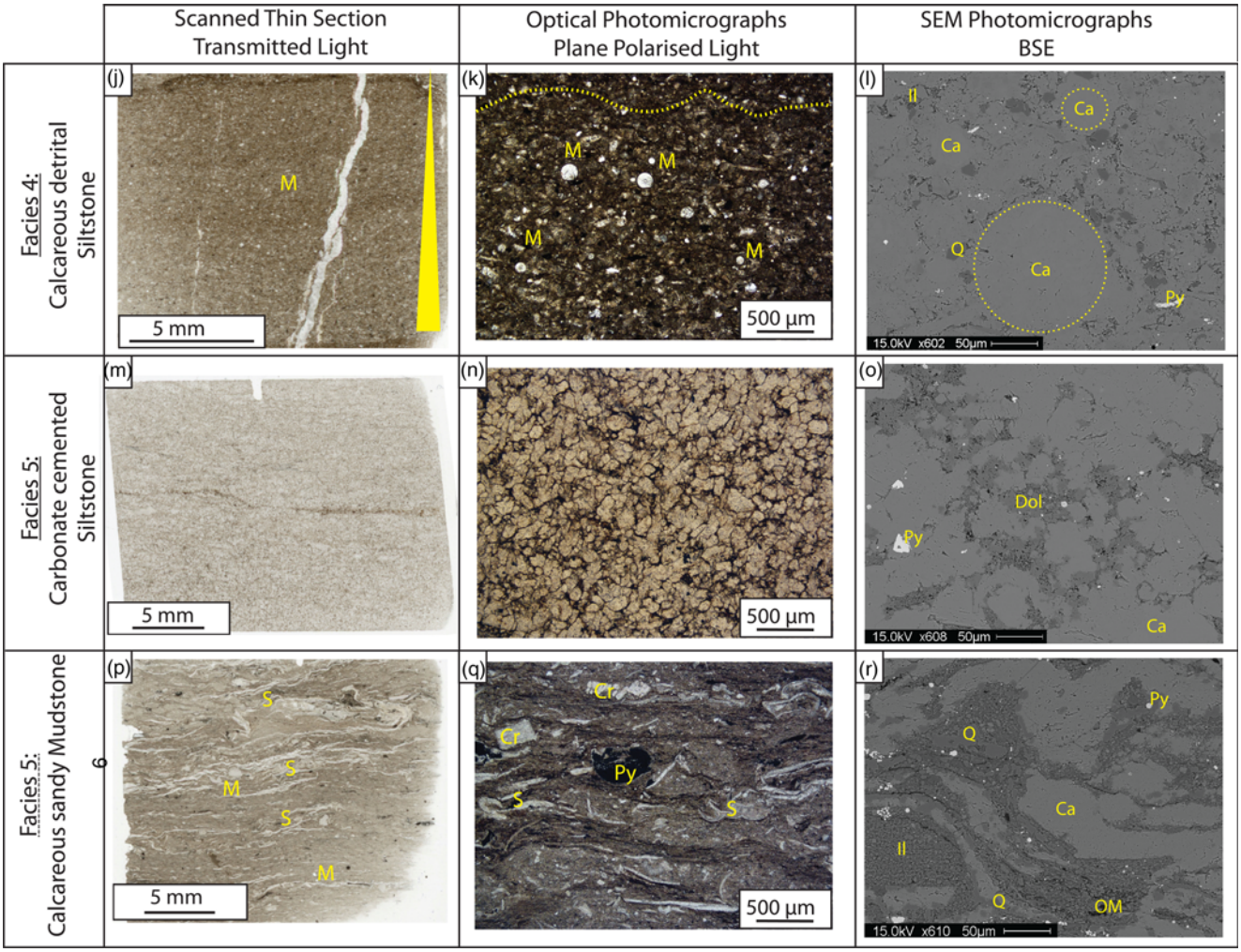

Fig. 4 *Continued.* (**j**) Scanned: MHD11_79 (99.4 m, Holkerian); coarse mudstone, calcareous, normal graded bed showing three smaller grading events (laminasets of light and dark bands); contains continuous, wavy, non-parallel laminations, microfossils common (M, foraminifera and sponge spicules, <250 µm). Fossils are most common and larger at the base of graded section. Pyrite associated in larger clumps with the coarser grained, more fossiliferous material. (**k**) Optical: MHD11_79 (99.4 m, Holkerian); coarse carbonate grains predominantly biogenic (microfossils) and detrital; comprises part of a light section of the smaller graded events; the change between light (coarser) and dark (finer) bands is highlighted. (**l**) SEM: MHD11_79 (99.4 m, Holkerian?) BSE SEM image; coarse mudstone (siltstone), calcareous, circular dashed line indicates perimeter of detrital biogenic microfossils, with calcite cement present as well as minor pyrite (framboids, <15 µm), quartz and illitic clay cements present. Facies 5: carbonate cemented siltstone. (**m**) Scanned: MHD11_20 (19.3 m, Pendleian); coarse mudstone, siltstone, calcareous, no obvious bedding or lamination present with homogeneous appearance, some linear features of darker material, dominant carbonate cement. Possible shell fragments (<1 cm in length but 10 µm in thickness). (**n**) Optical: MHD11_20 (19.3 m, Pendleian); pervasive carbonate (predominantly calcite) cement with minor clay material between. (**o**) SEM: MHD11_39 (30.6 m, Brigantian) BSE SEM image; coarse mudstone (siltstone), calcareous, homogeneous appearance, with dominant calcite cement, with secondary dolomite overgrowth, minor pyrite (framboidal and rhombs, <20 µm) and illitic clay filled pores. Facies 6: calcareous sandy mudstone. (**p**) Scanned: MHD11_76 (65.7 m, Asbian); sandy mudstone, calcareous (biogenic and detrital). Laminations are continuous wavy and parallel, some distorted around large grains (>600 µm). Large amount of fossiliferous material (S) including body fossils of ammonoids, bivalves or brachiopods, and crinoids. Numerous microfossils (M) including foraminifera and minor sponge spicules. Pyrite dispersed within clay laminasets and localized within large shell fragments. (**q**) Optical: MHD11_76 (65.7 m, Asbian); variation between clay-rich laminae containing minor detrital and biogenic carbonate (<70 µm) and carbonate-rich laminae containing abundant shell fragments (including crinoids, Cr) and detrital carbonate (<250 µm). Pyrite (Py) cementation associated with body fossil. (**r**) SEM: MHD11_76 (65.7 m, Asbian) BSE SEM image; sandy mudstone, calcareous (biogenic and detrital, <150 µm), with quartz (<50 µm), organic matter (<20 µm), framboidal pyrite and illitic clay.

calcareous claystone (Facies 1). Facies 1 represents the only facies with the potential for significant portions of the sediment to be derived from hemipelagic suspension, thus attesting to low rates of sediment supply within Facies Association A in contrast to other facies associations within the succession. The occurrence of thin beds of Facies 5 represents rare higher-energy debritic flows. The presence of soft-sediment folded beds in this facies association is indicative of sediment remobilization following deposition, caused by instability generated by gradients in a slope environment.

Facies Association B: slope dominated by low-density turbidites

This facies association comprises successions up to 15 m thick (Fig. 3), predominantly composed of calcareous mudstones (Facies 2), argillaceous mudstones (Facies 3), calcareous siltstones (Facies 4) and calcareous sandy mudstones (Facies 5). This facies association contrasts with Facies Association A by the absence of Facies 1, and by local presence of debrites (Facies 5). Deposition was predominantly via low-energy turbidites (T_0–T_8 of Stow &

Table 1. *Summary table of facies observed within the slope succession at Marl Hill*

	Physical sedimentological features		Biogenic features	Diagenetic features		
	Macro-scale	Micro-scale	Macro- and micro-scale	Macro- and micro-scale	Packages	Process interpretation
Facies 1: calcareous claystone; average TOC (wt%) 5.70 (3.70 to < 11.16)	Mid-grey to dark grey calcareous claystone. Occurs in homogeneous successions 0.001 to < 1.3 m; contains planar lamination, spaced < 5 mm (Fig. 4a)	Discontinuous and continuous planar parallel lamination, less common wavy or nonparallel lamination throughout. Laminations deflected around concretions. Discrete intervals of claystone lenses with elongate long axes 20 – 300 μm long, and short axes up to 50 μm long. Lenses are aligned to bedding, and their shapes are variable (Fig. 4b). Similar lenticular structures have been described by Schieber *et al.* (2007, 2010), Davies *et al.* (2012) and Könitzer *et al.* (2014) in other Paleozoic mud-rich successions	Minor bioturbation (BI = 2). Discrete intervals abundant whole ammonoid macro-fossils (<400 μm), whole microfossils, particularly foraminifera and spats (juvenile ammonoids; Fig. 4b). Rare, indeterminate fragmented shell material	Common calcite-filled veins (<1 mm thick). Carbonate (calcite and dolomite), clay and pyrite cements are common (Fig. 4c). Rare carbonate nodules (*c.* 2 cm)	0.001 to < 1.3 m homogeneous successions, typically observed in association with Facies 2, and rarely with Facies 4a and b, 5 and 6	The claystone lenses resemble those produced in flume experiments by 'soft', water-rich shale intraclasts that, following compaction, become flattened and develop a bedding-parallel long axis. The occurrence of these claystone intraclasts supports the notion that deposition was at least in part the product of gravity currents. The shelly material may also be transported, and homogeneous, ungraded successions of claystone containing detrital carbonate have previously been interpreted as the products of *en masse* deposition from gel or fluid mud layers, themselves derived from more dilute flows (McCave & Jones 1988; Talling *et al.* 2012) and equivalent to T_E of Bouma (1962), T_7–T_8 of Stow & Shanmugam (1980) and $T_{E\text{-}3}$ of Piper (1978) and Talling *et al.* (2012). However, the significant amount of well-preserved marine fauna may be indicative of hemipelagic suspension settling
Facies 2: calcareous mudstone; average TOC (wt%) 4.23 (1.21 to < 5.88)	Pale to dark grey calcareous mudstone. Occurs in beds 0.01 – 0.1 m thick. Beds normally graded as defined by a decrease upward in shell fragment size and abundance (Fig. 4d). Lags of massive pyrite clasts up to 1 cm sometimes occur at the bases of normally graded beds. Planar laminated (Fig. 4d), at a spacing < 50 mm. Rare, pale grey lithoclasts of mudstone (<2 cm; sub-angular to sub-rounded), typically associated near the base of bed. Rarely wavy non-parallel bedding and convoluted laminations present	Continuous parallel laminations, and less common discontinuous, wavy lamination. Laminae are deflected around nodules (Fig. 4d). Clay-rich lenses similar to those in Facies 1 are common throughout (Fig. 4d and e). Lens long axes are 20 – 600 μm long, and short axes up to 100 μm long	Minor bioturbation (BI = 1), although a single 5 cm thick interval with BI = 3 occurs in the dark grey mudstone. Common indeterminate fragmented shell material occurs in localized packages (Fig. 4e). Rarely whole disarticulated crinoid ossicles, fragmented bivalve, brachiopod and ammonoid fossils (<500 μm). Microfossils, including whole foraminifera tests and fragments of sponge spicule are common, locally associated with ammonoids	Common carbonate and phosphate nodules (*c.* 3 cm), especially in packages <1 m thick of dark grey mudstone. Less common are pyrite and siderite nodules and massive pyrite. Common calcite-filled veins, rarely stained red. Common carbonate (calcite and dolomite), clay and pyrite cements (Fig. 4f)	Beds stack into fining-upwards and more rarely coarsening-upwards successions 0.4 to < 1.5 m thick, but up to 12 m in one instance. Typically associated with Facies 1, 3, 4 and 6	The normally graded beds are characteristic of waning density-flow (turbidite) deposits, and correspond to the $T_{E\text{-}1}$, $T_{E\text{-}2}$ and $T_{E\text{-}3}$ subdivision of Piper (1978) and T_3, T_6 and T_7 subdivision of Stow & Shanmugam (1980). Further evidence of traction-driven flows within the facies includes the presence of claystone lenses, which represent semi-lithified mudstone, pyrite and mudstone lithoclasts, and fragmented shell material. As with Facies 1, significant contribution of sediment from hemipelagic suspension settling cannot be entirely ruled out

(continued)

Table 1. (Continued)

	Physical sedimentological features		Biogenic features	Diagenetic features		
	Macro-scale	Micro-scale	Macro- and micro-scale	Macro- and micro-scale	Packages	Process interpretation
Facies 3: argillaceous mudstone; average TOC (wt%) 3.81 (3.30 to < 4.53)	Mid-grey argillaceous mudstone (Fig. 4g). Occur in beds 0.1 to < 1.5 m thick; predominantly massive, occasionally normally graded. Planar laminae, at a spacing < 50 mm	Discontinuous wavy laminations, nonparallel or parallel, with less common discontinuous planar parallel laminations (Fig. 4h). Clay-rich lenses with elongate long axes 20 – 800 μm long, and short axes up to 100 μm long (similar to those described in Facies 1) are very common (Fig. 4h and i)	Minor bioturbation (BI = 2). Rare indeterminate fragmented shell material and fragmented ammonoid fossils (<500 μm). Common microfossils, particularly whole foraminifera tests (Fig. 4h)	Common carbonate (calcite, dolomite and/or siderite), clay and pyrite cements (Fig. 4i), with gypsum coating on surface of samples. Rare carbonate nodules (*c.* 1 cm) and calcite-filled veins (<3 cm thick)	Beds organized into *c.* 6 m thick fining-upwards successions. Gradational contacts with Facies 2 and Facies 4b	As with Facies 2, the normally graded beds are characteristic of waning density-flow (turbidite) deposits, and correspond to T_{E-1}, T_{E-2} and T_{E-3} subdivision of Piper (1978) and T_3, T_6 and T_7 subdivision of Stow & Shanmugam (1980). The greater proportion of argillaceous sediment suggests that the source of the sediment was more argillaceous and less carbonate rich compared with Facies 2
Facies 4: calcareous siltstone; average TOC (wt%) 3.58 (1.21 to < 4.98)	Pale to mid-grey siltstone. Beds typically 0.01 to < 0.4 m thick and are normally graded with sharp or erosive bases with shell lags at their bases (Fig. 4j and k). Ripple cross-lamination occurs in one instance at the base of a bed. Horizons of convoluted lamination are common, as are intraclasts of coarse shell material. Laminae are deflected around nodules. Occasional pale grey homogeneous structureless beds (0.15 to < 0.5 m) occur (Fig. 4m and n)	Continuous, wavy nonparallel laminations are common (Fig. 4k). Rare clay-rich laminae, discontinuous planar or wavy parallel laminations and nodules or spheres of organic material up to 100 μm occur in otherwise homogeneous beds	Rare bioturbation (BI = 0 to < 1). Common indeterminate fragments of shell material (<5 cm). Rare fragmented crinoid, bivalve and corals. Common microfossils, including whole foraminifera tests and sponge spicule fragments (Fig. 4k). Within homogeneous beds (Fig. 4n) no preserved bioturbation present, and rare, recrystallized, fragmented ammonoids occur	Common calcite-filled veins and rare carbonate nodules. Calcite, dolomite, clay and iron sulphide (pyrite and possibly marcasite) cements (Fig. 4l). Within homogeneous beds pervasive calcite and dolomite cements are present (Fig. 4o). Calcite veins (<1 cm thick) and partially filled fractures of calcite, siderite and organic material occur. Nodules of phosphate, calcite, dolomite and pyrite (*c.* 2 cm) occur. Rare massive pyrite	Thin, 0.1 to < 0.6 m thick successions. Associated with Facies 2, 5, 6, and more rarely Facies 1 and 3	The occurrence of normally graded beds with erosive bases, and pyritic silt shell lags, is typical of waning density-flow (turbidite) deposits. The siltstone grain size and presence of ripple cross-lamination clearly indicates that these are higher energy flows than Facies 1–3. Facies 4 corresponds to T_{C-D} of Bouma (1962), T_D and T_{E-1} of Piper (1978) and Talling *et al.* (2012) or T_0 to T_2 of Stow & Shanmugam (1980). The convolute lamination attests to rapid dewatering of the sediment, probably owing to rapid deposition of sediment. Where the facies appears homogeneous and structureless, significant diagenetic overprinting from carbonate cementation has obscured the original depositional fabric
Facies 5: calcareous sandy mudstone; average TOC (wt%) 1.57	Pale to mid-grey sandy mudstones predominantly composed of detrital and bioclastic carbonate material (Fig. 4p). Beds 0.05 – 0.5 m thick. Beds display erosive bases, weak normal or reverse grading, and contain dispersed mudstone lithoclasts (0.5 to < 2 cm, sub-rounded to sub-angular)	Highly disturbed beds 1 – 20 cm thick containing abundant wavy laminations that are discontinuous or continuous, and parallel or nonparallel (Fig. 4p and q)	Bioturbation is common throughout (BI = 2 to < 4), but intense (BI = 4) in shelly horizons (Fig. 4q). Shell fragments are numerous, locally occurring in packages <15 cm thick and containing 20% shell debris, including fragmented crinoid ossicles, rugose corals and bivalves (Fig. 4q). Common fragmented ammonoids, coral, bivalves and brachiopods, with whole foraminifera, radiolarian and sponge spicules	Calcite-filled veins. Common calcite and dolomite, clay and pyrite cements (Fig. 4r). Common massive pyrite and nodules of pyrite throughout	Packages 0.4 m to < 4 m thick. Typically associated with Facies 2, 4 (a and b) and 6	The presence of weak normal and inverse grading, and the abundance of scattered lithoclasts and carbonate allochems supported by a claystone matrix, is indicative of deposition *en masse* by low-strength cohesive debrites (e.g. McIlreath & James 1978; Talling *et al.* 2012; Lazar *et al.* 2015*b*). This lithofacies corresponds to D_{M-1} of Talling *et al.* (2012)

Facies 6: matrix-supported carbonate conglomerate	Pale to dark grey calcareous sandy mudstone matrix predominantly composed of detrital and bioclastic carbonate material (similar to Facies 5). The matrix supports olive-coloured sub-rounded to angular polymict clasts of wackestone and floatstone 0.001 – 0.27 m in diameter. Clasts occur in massive, ungraded chaotic successions 3 to < 5 m thick, although the largest clasts are locally present at the bases of beds. Lesser quantities of mudstone clasts up to 0.05 m occur. Clast:matrix ratio is *c.* 6:1. Shear fabrics occur at the bases of beds	Not studied	Bioturbation (BI = 3) is common throughout the matrix. Fragments of shell material up to 0.08 m occur commonly in the matrix, including rugose coral corallum and disarticulated crinoid ossicles. Within the wackestone to floatstone clasts numerous shell fragments are present, including crinoid ossicles and corals	Calcite-filled veins up to 1.4 cm in diameter are common. Pyrite is associated with the calcite-filled fractures and is also found in massive and nodular form	Massive, ungraded successions 3 to < 5 m thick. The facies is associated with Facies 2 (calcareous mudstones)	Metre-thick massive successions of sandy mudstone supporting clasts up to boulder size, and displaying shear-fabrics at the bases, are characteristic of the products of cohesive debris flows (i.e. debrites; Talling *et al.* 2012). Facies 6 is equivalent to moderate- or high-strength debris flows, D_{M-2} of Talling *et al.* (2012). The large amount of disarticulated crinoid ossicles and rugose coral corallum suggests a depositional site near a site of carbonate productivity (i.e. carbonate shelf, or waulsortian mudmound on a slope)

It should be noted that degree of bioturbation is recorded using a 0 – 5 scale, from no visible burrows to no remnant bedding when a rock interval is fully homogenized (after Lazar *et al.* 2015*b*).

Shanmugam 1980). As with Facies Association A, the presence of mudstone lenses suggests that some of the sediment was partially lithified prior to deposition, and the presence of slumped horizons is indicative of deposition on a gradient. The absence of Facies 1 suggests that deposition rates were higher than in Facies Association A, resulting in the dilution of contributions from hemipelagic suspension settling. Overall, this facies association represents the lower portion of a slope that is actively receiving both carbonate and clastic sediment from the shelf.

Facies Association C: slope dominated by debrites

This facies association comprises successions up to 10 m thick (Fig. 3), predominantly composed of matrix-supported carbonate conglomerate (Facies 6) and calcareous mudstone (Facies 2). Facies Association C represents the alternation of deposition from moderate- to high-strength cohesive debris flows (D_{M-2}, Talling *et al.* 2012) and low-energy turbidites (T_3, T_6 and T_7; Stow & Shanmugam 1980). The polymict wackestone and floatstone lithology of the clasts in Facies 6 and the presence of biogenic material indicative of fully open-marine conditions suggest that the source of material was a low-energy carbonate-rich shelf below the storm wave base.

Facies association succession, depositional model and sequence stratigraphy

Metres 125 – 64 of the core are characterized by three whole coarsening-up successions. Metres 115 – 93 (sequence I; Fig. 3) record a change from a sediment-starved slope to a slope dominated by low-density turbidites. Metres 93 – 78 (sequence II; Fig. 3) record a change from a sediment-starved slope through a slope dominated by low-density turbidites to a slope dominated by debrites. Metres 78 – 64 (sequence III; Fig. 3) record a change from a sediment-starved slope to a slope dominated by low-density turbidites. The succession from 64 to 5 m (sequence IV; Fig. 3) is represented entirely by a sediment-starved slope.

The evidence of significant proportions of slumping and sliding as well as the occurrence of periodic inputs via low-density turbidites and debrites suggest that this is a slope succession (McIlreath & James 1978; Shanmugam 2000; Stow & Mayall 2000). Slope successions are inherently progradational (Patruno *et al.* 2015), with the thickness between basin floor sediment and shelf top sediments representing the (minimum) height of the slope clinoforms. No transition from basin floor to shelf top sediments is observed within the succession, suggesting that the slope clinoform was at least of the order of 120 m (accounting for decompaction). This thickness is within the range of 100 – 1000 m usually indicated for basin-margin clinoforms (Patruno *et al.* 2015), and, combined with the carbonate-rich nature of the sediment, strongly implies that it was a basin-margin, rather than delta-front, slope succession.

The lower three cycles (Cycles I–III) represent deposition on the slope with gradually increasing proximity to active sedimentation on the shelf. The initial slope conditions were relatively sediment-starved (Facies Association A; Fig. 5) because shorelines were distant from the shelf margin and active carbonate productivity and clastic sediment delivery occurred far away from the slope. Whilst on the slope, hemipelagic suspension settling of fine, organic-rich mud may have dominated. Episodic, storm-generated or river-effluent-generated density currents distributed fine-grained sediment across the shelf and onto the slope. Shelf-generated density currents may have bypassed the upper slope and deposited on the lower slope, or material deposited on the upper slope may have been remobilized via slumps and slides, transforming into turbidites and rare debrites, which deposited on the lower slope. We hypothesize

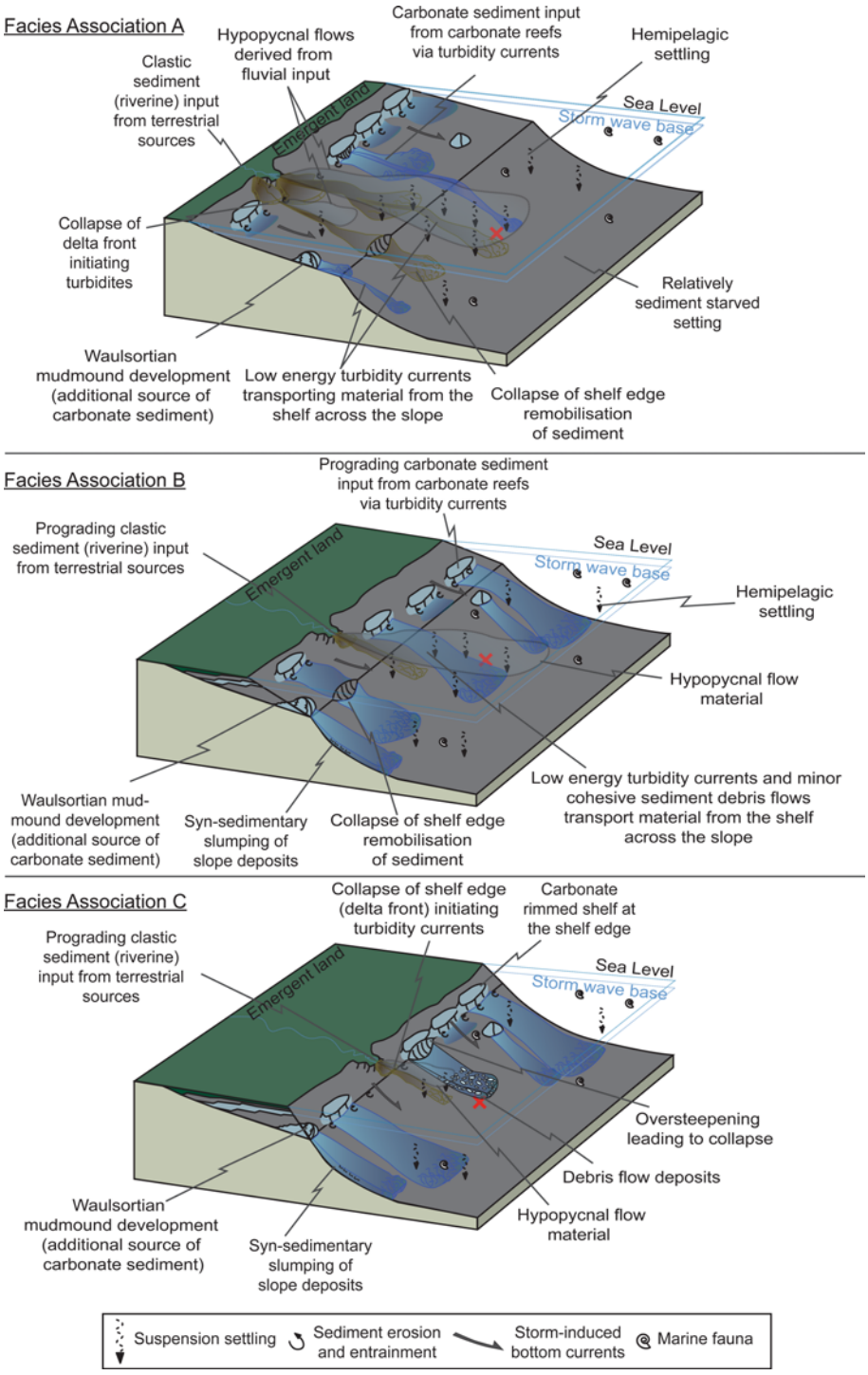

Fig. 5. Schematic 3D block models for the basin during the deposition of Facies Associations A, B and C, showing the changes in sedimentation on the slope as a result of changes on the prograding shelf, with the location of the marl hill core highlighted by red cross (not to scale).

that the lenses (shale lithic clasts) within the succession represent reworked, partially lithified upper slope sediments.

As shorelines prograded towards the shelf margin, the slope received increasing volumes of coarser sediment (Facies Association B; Fig. 5), largely delivered via storm-derived and river-effluent-derived density currents. In Cycle II, continued progradation of the shoreline resulted in oversteepening at the shelf margin and large-scale collapse of partially cemented carbonate-rich shelf sediments down the slope, resulting in the deposition of calcareous sandy mudstones and carbonate conglomerates on the lower slope (Facies Association C; Fig. 5). All three cycles are overlain sharply by sediment-starved slope sediments of the following cycle.

Cycles I–III, representing shoreline progradation followed by rapid regression across the contemporaneous shelf, occur through the Arundian to Asbian (Fig. 3; Waters *et al.* 2007), implying durations for each cycle of the order of *c.* 4 myr. Shoreline progradation occurs when sediment supply outpaces the rate at which accommodation is generated on the shelf, which may be during relative sea-level stillstand or rising relative sea-level (normal regression) or during relative sea-level fall (forced regression; Mitchum *et al.* 1977; Vail *et al.* 1977; Howell & Flint 1996; Catuneanu 2002; Gawthorpe *et al.* 2003). The duration of these cycles suggests that they represent sequence scale (third order; 1 – 2 myr) changes rather than stacked sequences (second order; 9 – 10 myr) or parasequence scale (fifth order; 0.01 – 0.02 myr; Mitchum & Van Wagoner 1991).

The upper succession (Cycle IV) from 64 to 5 m consists entirely of starved slope sediments (Facies Association A; Fig. 3), and represents an extended period of little sediment delivery to the

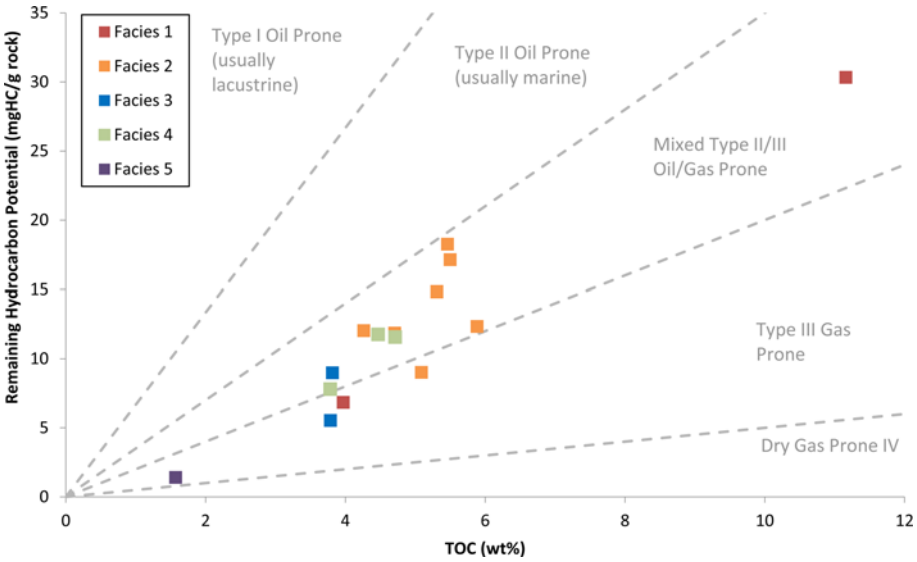

Fig. 6. Kerogen quality plots indicating the kerogen type of the remaining total organic matter (*y*-axis corresponds to S2 from Rock-Eval™). The majority of samples are composed of mixed type II–III kerogens; four samples (from Facies 1, 2, 3 and 5) demonstrate type III kerogens.

slope, with carbonate and clastic sediments trapped on the shelf. The succession represents of the order of *c.* 5 myr of sedimentation, and implies the shelf was largely flooded for this period, with neither clastic nor carbonate shallow marine sedimentation being able to prograde across the shelf. The succession notably overlies the *Goniatites globostriatus* (B_{2b}) 'Marine Band' (Fig. 3). Fossiliferous horizons, termed 'marine bands', allow correlation across the Pennine Province (Ramsbottom 1973, 1978, 1979; Holdsworth & Collinson 1988; Waters & Condon 2012). Marine bands are interpreted to represent condensation associated with maximum flooding surfaces during major transgressions (third-order cycles; Mitchum & Van Wagoner 1991), and in the Namurian have been linked to possible fluctuations in Gondwanan ice-sheet dynamics and inferred Milankovitch orbital forcing (Isbell *et al.* 2003; Frank *et al.* 2008; Rygel *et al.* 2008; Stephenson *et al.* 2010; Waters & Condon 2012; Könitzer *et al.* 2014; Gross *et al.* 2015). The occurrence of the B_{2b} at the base of Cycle IV can be used to infer that the cycles (I, II, III and IV) observed within the core could represent relative sea-level cycles similar to those observed by Ramsbottom ('mesothems' D2 to D6b; Ramsbottom 1973, 1981) and regressions observed by Ross & Ross (1987).

The variation in sedimentation style that is observed within the core at the boundary between Cycle III and Cycle IV (Fig. 3) is likely to have been effected by the changes in tectonism that the basin experienced at the time as well as the fluctuations in sea level (Fraser & Gawthorpe 2003; Haq & Schutter 2008). During EC3 (Chadian to Holkerian; Cycles I–III) the basin experienced a phase of active synrift tectonism that was associated with the reactivation of extensional faults, whereas during EC4 (late Holkerian to mid-Asbian) and EC6 (early to mid-Brigantian) post-rift periods occurred. These tectonic changes, in combination with sea-level variation, therefore resulted in a more stable and uniform succession within the studied core for the duration of Cycle IV.

By defining a slope depositional setting for the succession (Fig. 5) it is possible to interpret the smaller scale sedimentological features observed, such as mudstone lenses and organic matter variations, within that context.

Origin and significance of mudstone lenses in the slope succession

Clay-rich mudstone lenses, referred to as lenticular fabric, are common within both claystone and mudstone lithofacies within the Marl Hill succession. The lenses range from 50 to 800 μm, with smaller lenses found in Facies 1 (calcareous claystone) compared with Facies 3 (argillaceous mudstone). They appear elongated in shape, have tapering uneven edges with no apparent borders (i.e. no appearance of burrow linings) and show apparent alignment along bedding (Fig. 4b, e and h). Lenticular fabric has been observed in a wide range of mud-rich settings and various processes or sources for this fabric have been proposed, including bioturbation, faecal pellets or re-sedimented shale clasts (e.g. Wignall 1994; Rohl *et al.* 2001; Schieber *et al.* 2007; Gabbott *et al.* 2010; Davies *et al.* 2012; Ghadeer & Macquaker 2012; Könitzer *et al.* 2014; Schieber 2016*a*). The lenses observed within the succession are unlikely to be produced by bioturbation or faecal pellets owing to their elongated profile, the shape and distinction of the lens edges, and alignment with bedding as well as the wide range in size. Instead, the lenses resemble those produced in flume experiments by 'soft' water-rich (75%) shale intraclasts (Schieber *et al.* 2010; Schieber 2016*a*). Similar features have been identified within other Paleozoic successions from both shelf (Schieber *et al.* 2007, 2010; Davies *et al.* 2012) and basin floor successions (Könitzer *et al.* 2014, 2016; Schieber 2016*b*).

It has been suggested that the mud intraclasts within the Marl Hill succession were derived from partially lithified, upper to mid-slope sediments, owing to the fine grain size of these intraclasts (McIlreath & James 1978; Stow & Piper 1984) and the complex basin morphology of the Bowland Basin (half-graben within a shallow epicontinental seaway with long-lived palaeogeographical barriers; Fig. 1) reducing the likelihood of long distance transport from either riverine or shelf processes (Fraser & Gawthorpe 1990; Davies 2008; Waters *et al.* 2009, Woodcock & Strachan 2002). It is important to note that flume experiments conducted by Schieber (2016*a*) concluded that transport of 'soft' mud-rich clasts could occur over distances of the order of thousands of kilometres; therefore, it is not possible to entirely discount contribution from riverine transport or shelf processes in the source of mud intraclasts within the succession.

The presence of mud intraclasts within a mud-rich slope succession, such as Marl Hill, is significant as not only does it provide evidence of traction, even within the most fine-grained facies, but also it demonstrates that the succession is not purely the product of hemipelagic settling of material even at times of lowest sediment accumulation rates on the contemporaneous shelf (Facies Association A; Fig. 5). In addition, it demonstrates that the process of erosion, transport and deposition of soft water-rich mud clasts can occur within a slope environment as well as both shelf and basin floor successions.

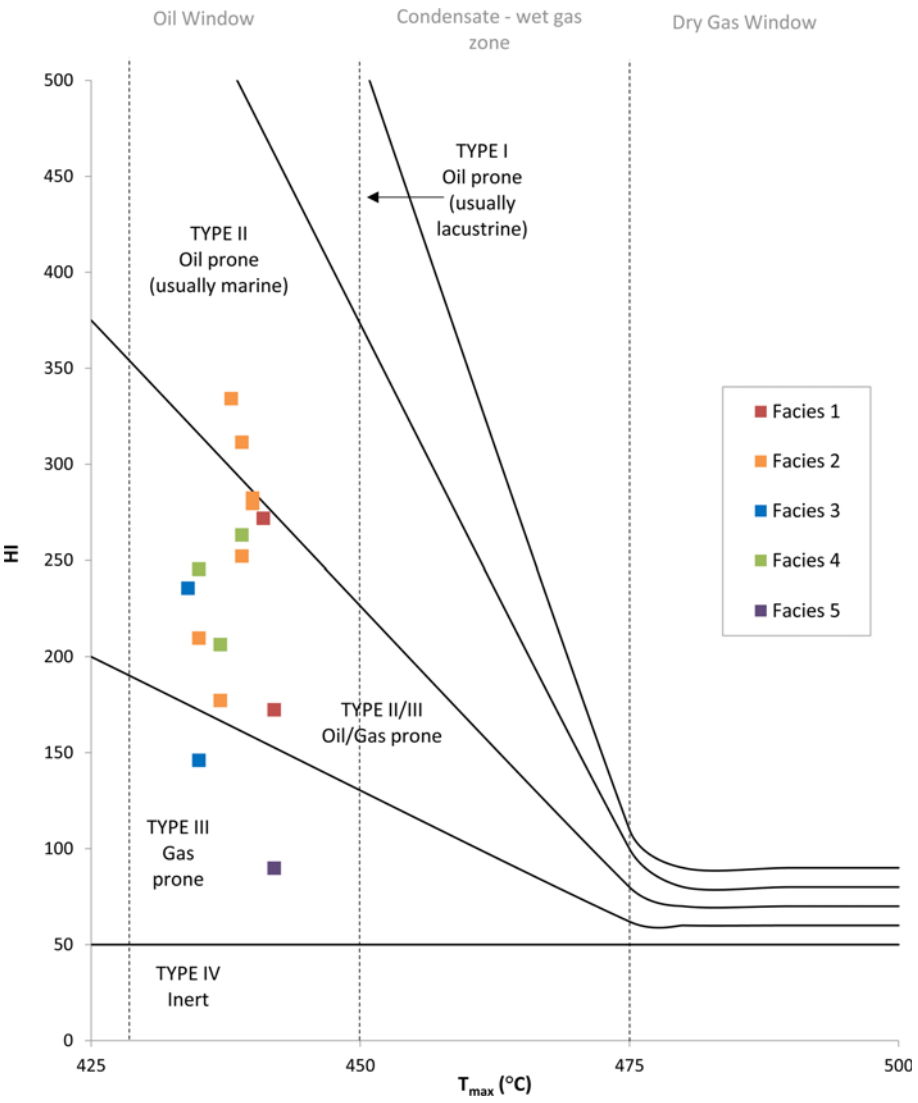

Fig. 7. Plot of T_{max} and HI showing maturity and kerogen type (a modified van Krevelan plot). The T_{max} (*x*-axis) indicates the maturity the samples have reached and the black dotted lines indicate oil, condensate gas and dry gas windows. The majority of samples plot as mixed type II–III kerogens, two samples (Facies 2) plot as type II and two samples (Facies 3 and 5) plot as type III. All samples plot within the oil window.

Distribution of organic matter in the slope succession

Organic matter (OM) content within the succession is highly variable (1.05 to < 11.16 wt% TOC). Within the succession between 64 and 5 m (Facies Association A, Cycle IV, Bowland Shale Formation; Fig. 3) detailed sampling allows the organic characteristics of single lithofacies to be established. Calcareous claystones (Facies 1) contain the highest organic matter content (average 5.70 wt%; 3.70 to < 11.16 wt.%; $n = 6$), with Facies 2, calcareous mudstones (average 4.23 wt%; 1.21 to < 5.88 wt%; $n = 15$), Facies 3, argillaceous mudstone (average 3.81 wt%; 3.30 to < 4.53 wt%; $n = 6$), Facies 4, calcareous siltstones (average 3.58 wt%; 1.21 to < 4.98 wt%; $n = 8$) and Facies 5, calcareous sandy mudstone (average 1.57 wt%; $n = 1$), showing a broad trend of decreasing organic matter content with increasing grain size.

The depositional processes that created each facies were probably instrumental in controlling the nature and content of the facies-specific organic matter (Table 1). The lithofacies with the greatest contribution from hemipelagic settling (Facies 1) show the greatest enrichment of organic matter. RockEval™ data (Figs 6 and 7; Facies 1) suggest kerogen type II–III, indicating a mixed marine and terrestrial source of organic matter. Mixed type II–III kerogen possibly resulted from the clay-rich lenses observed within the facies that contributed a reworked type III kerogen signature to the organic matter from hemipelagic settling (typically) type II kerogen.

The lithofacies primarily deposited as a result of low-density turbidite deposits, Facies 2, 3 and 4, consist of mixed type II–III kerogen. Calcareous mudstones (Facies 2) differ from argillaceous mudstones (Facies 3) in the nature of the organic matter they contain, when observed using back-scattered electron (BSE) SEM (Fig. 4). Argillaceous mudstones contain predominantly fragmentary 'solid' OM, inferred to originate from more terrigenous sources (Type III kerogen; Fig. 4i), although calcareous mudstones contain predominantly amorphous OM (OM that aligns along bedding and distorts around grains), inferred to originate from marine sources (Type II kerogen; e.g. Hackley & Cardott 2016; Newport *et al.* 2016; Fig. 4f). Organic geochemical parameters (i.e. HI, S_2) also suggest a contrast in kerogen type between the two facies, where argillaceous mudstone plots close to or within Type III kerogen and calcareous mudstone plot close to or within Type II kerogen (Figs 6 and 7; Table 2). This suggests that sediment and OM for the argillaceous mudstones were derived from a predominantly terrestrial clastic source such as riverine input, and the sediment and OM for the calcareous mudstones were derived from a more marine carbonate source such as shelf carbonate reefs or isolated carbonate build-up (i.e. mudmounds; Fig. 5).

The lithofacies primarily deposited as a result of low-strength, cohesive debrites, calcareous sandy mudstone (Facies 5), contain the lowest TOC content of all facies measured (average 1.57 wt %). RockEval™ data for Facies 5 suggest presence of Type III kerogens with low HI values and relatively high OI values (90 and 13, respectively; Fig. 7; Table 2). These geochemical data suggest a predominantly terrestrial origin for the organic matter within Facies 5, contrasting with the sedimentological evidence, such as

Table 2. *Organic geochemical data from all facies: TOC and RockEval™ primary and secondary parameters (S1, S2, S3, T_{max}, HI and OI)*

Sample number	Depth (m)	European Substage	TOC (wt%)	Facies	S1 (mg g^{-1})	S2 (mg g^{-1})	S3 (mg g^{-1})	T_{max} (°C)	HI (mg HC g^{-1} TOC)	OI (mg CO_2 g^{-1} TOC)
MHD11_2	6.2	Pendleian	3.81	3	1.2	9.0	0.7	434	236	19
MHD11_5	8.1	Pendleian	3.67	3	–	–	–	–	–	–
MHD11_7	9.1	Pendleian	4.53	3 (minor 1 & 4)	0.9	7.0	0.4	425	156	9
MHD11_8	9.9	Pendleian	3.76	3	–	–	–	–	–	–
MHD11_11	12.2	Pendleian	3.59	2	–	–	–	–	–	–
MHD11_14	15.6	Pendleian	3.79	3	0.7	5.5	0.3	435	146	9
MHD11_17	18.3	Pendleian	3.37	2	–	–	–	–	–	–
MHD11_20	19.3	Pendleian	4.47	4	1.2	11.8	0.4	439	263	8
MHD11_26	20.9	Pendleian	5.46	2	1.4	18.3	0.4	438	334	7
MHD11_27	22.1	Brigantian	4.98	2 (minor 1 & 4)	1.0	9.9	0.3	435	199	7
MHD11_29	23.4	Brigantian	4.71	2	1.0	11.9	0.3	439	252	6
MHD11_32	25.9	Brigantian	5.31	2	1.4	14.8	0.3	440	280	6
MHD11_35	27.5	Brigantian	3.30	3	–	–	–	–	–	–
MHD11_37	29.7	Brigantian	3.67	2	–	–	–	–	–	–
MHD11_41	31.6	Brigantian	5.50	2	1.7	17.1	0.4	439	311	7
MHD11_47	37.5	Brigantian	4.26	2	1.1	12.0	0.4	440	282	10
MHD11_48	38.8	Brigantian	3.43	2	–	–	–	–	–	–
MHD11_57	46.2	Brigantian	3.78	4	0.8	7.8	0.4	437	206	10
MHD11_59	48.8	Brigantian	4.71	4	1.2	11.6	0.5	435	245	11
MHD11_62	53.1	Brigantian	5.88	2 (minor 1)	1.5	12.3	0.4	435	210	7
MHD11_64	55.3	Brigantian	3.34	2	–	–	–	–	–	–
MHD11_66	56.9	Brigantian	1.26	4	–	–	–	–	–	–
MHD11_69	60.1	Brigantian	3.70	2, 4 & 1	0.7	4.9	0.4	441	132	10
MHD11_71	62	Brigantian	5.09	2	1.0	9.0	0.4	437	177	8
MHD11_72	62.8	Brigantian	11.16	1	2.3	30.3	0.4	441	272	3
MHD11_73	63.7	Asbian	1.57	5	0.2	1.4	0.2	442	90	13
MHD11_75	65.1	Asbian	3.97	1	0.8	6.8	0.3	442	172	7
MHD11_78	94.2	Holkerian	1.21	2, 4	–	–	–	–	–	–

carbonate allochems, suggesting an origin from slope instability and collapse of carbonate build-ups (Table 1; Fig. 4). However, the mineral matrix can have a significant influence on the RockEval™ kerogen typing, particularly with sediments consisting of less than 2 wt% organic carbon, such as Facies 5, leading to uncertainty in the data. Hydrocarbon retention on mineral grains can result in a reduction in the HI, and thermal decomposition of small amounts of carbonate during analysis can increase the OI by contributing additional carbon dioxide (Espitalié *et al.* 1980; Katz 1983; Dembicki 2009). Another explanation for the Type III signature for this facies is a mixture of Type II, III and IV kerogens (Dembicki 2009). Type IV (inertinite) kerogen would contribute to the TOC value but not significantly to the S_2 values, therefore lowering HI values reported; however, from Type IV kerogens one would also expect an increase in OI values above that observed (Fig. 6; Table 2). Another consideration when using RockEval™ data to type kerogens present is the maturity of the sediments, as Type I, II and III RockEval™ indices evolve with maturation of the respective hydrocarbons (Dembicki 2009). All samples taken from the Marl Hill succession plot within the oil window of the modified van Krevelen plot, indicating that they are oil-mature, with average T_{max} values of 438°C (Fig. 7; Table 2), and thus it is appropriate to use RockEval™ indices to estimate kerogen type.

Within Facies Association A, the minimum TOC value of *c.* 3.70 wt%, observed for Facies 1, may reflect the background organic matter supply and preservation on the sediment-starved slope setting where the minimum amount of sediment dilution occurs, whereas the minimum TOC value of *c.* 1 wt% for Facies 4 may reflect the background organic matter supply and preservation on the sediment-starved slope setting where the maximum amount of sediment dilution occurs. Variations can be observed in organic matter content between facies associations; Facies Association A (TOC average 3.95, lowest 1.05 and highest 11.16 wt%) and Facies Association B (TOC average 3.54, lowest 1.21 and highest 9.55 wt %) show a relative enrichment in Facies Association A relative to Facies Association B of the order of 1 wt%. Variation can also be observed in the type of kerogens within the facies associations, with Facies Association B consisting of a higher degree of Type III material than Facies Association A; this may be due to the nature of the prograding shelf contributing a more significant signature from terrestrial organic material (Fig. 5). Variation in the type and quantity of organic matter between facies associations is significant, as it allows the prediction of organic matter content and type to be made based on the relative sea level (i.e. sequence stratigraphic framework) of a slope succession.

Conclusions

(1) Six lithofacies, comprising calcareous claystone, calcareous mudstone, argillaceous mudstone, calcareous siltstone, calcareous sandy mudstone and matrix-supported carbonate conglomerate, are identified in core MHD11. Depositional processes in all are dominated by turbidites and/or debrites. There are three facies associations: a sediment-starved slope, a slope dominated by turbidites and a slope dominated by debrites. Conditions of sediment starvation on the slope occurred during flooding of the contemporaneous shelf, when shorelines and loci of active clastic and carbonate sedimentation were furthest away from the slope. Nevertheless, active sedimentation did occur on the slope at this time, via dilute turbidites, derived from storm-generated or river-effluent-generated density flows that traversed the shelf, or via slumps and slides on the upper slope that transformed into density flows. The transition towards a slope dominated by turbidites and then debrites occurred during normal or forced shoreline progradation towards the shelf margin. Large clasts of carbonate that occur within the slope dominated by debrites facies association are interpreted as the deposits of collapsed shelf-edge carbonates at the time of maximum shoreline progradation.

(2) The Bowland Shale Formation largely consists only of sediment-starved slope sediments, which resulted from an extended period (*c.* 5 myr) of low quantities of sediment delivery to the slope, with carbonate and clastic sediments trapped on the shelf, owing to a largely flooded shelf.

(3) The presence of mud intraclasts within a mud-rich slope succession provides evidence of traction, even within the most fine-grained facies, rather than the sediment being purely the product of hemipelagic settling. The presence of mud intraclasts also demonstrates that the process of erosion, transport and deposition of soft water-rich mud clasts can occur on a slope, as well as shelves and basin floors, as previously described.

(4) The sediment-starved slope succession is dominated by Type II kerogen, whereas the slope dominated by low-density turbidites is dominated by Type III kerogen. The difference is interpreted to represent a greater contribution from (reworked) deposits of marine hemiplegic settling on the sediment-starved slope, and a greater contribution from terrestrially derived organic material on the slope dominated by turbidites.

(5) This study suggests that mud-dominated lower slope settings are largely active depositional sites, where there is consistent evidence for sediment traction. Additionally, the composition and texture of basin slope mudstones, as well as organic content, vary predictably as a function of shelf processes linked to relative sea-level change.

(6) Variation in composition and texture of slope mudstones, as well as organic matter concentration and type, has been observed within the core studied. This approach can be applied within a basin with a pre-existing sequence stratigraphic framework as a result of greater data availability, and will facilitate predictions of porosity, permeability, mechanical properties, TOC and kerogen type.

(7) In contrast to previous assumptions, this study demonstrates that mud-dominated lower basin slopes are active depositional sites resulting in a wide range of deposits from both turbidity currents and debris flows.

Acknowledgements The authors thank M. Jones at Newcastle University and G. Hansen at APT Norway for analytical services provided, as well as the British Geological Survey for the loan of material. S.M.N. thanks L. Newport for the many discussions relating to this paper. E.H. publishes with the approval of the Executive Director of the British Geological Survey, Natural Environment Research Council.

Funding S.M.N. thanks NERC EAO DTP for provision of funding (NE/L002469/1) for this PhD research.

Scientific editing by Adrian Hartley

References

Aitkenhead, N., Bridge, D.McC., Riley, N.J. & Kimbell, S.F. 1992. *Geology of the Country around Garstang. Memoir for 1:50 000 geological sheet 67 (England & Wales)*. British Geological Survey. HMSO, London.

Andrews, I.J. 2013. *The Carboniferous Bowland Shale Gas Study: Geology and Resource Estimation*. British Geological Survey for Department of Energy and Climate Change, London.

Aplin, A.C. & Macquaker, J.H.S. 2011. Mudstone diversity: Origin and implications for source, seal, and reservoir properties in petroleum systems. *AAPG Bulletin*, **95**, 2031–2059, https://doi.org/10.1306/03281110162

Arthurton, R.S., Johnson, E.W. & Mundy, D.J.C. 1988. *Geology of the Country Around Settle. Memoir for 1:50 000 geological sheet 60*. British Geological Survey. HMSO, London.

Bohacs, K.M., Lazar, O.R., Demko, T.M., Bohacs, K.M., Lazar, O.R. & Demko, T.M. 2014. Parasequence types in shelfal mudstone strata – Quantitative observations of lithofacies and stacking patterns, and conceptual link to modern depositional regimes. *Geology*, **42**, 131–134, https://doi.org/10.1130/G35089.1

Bouma, A.H. 1962. *Sedimentology of Some Flysch Deposits: A Graphic Approach to Facies Interpretation*. Elsevier, Amsterdam/New York.

Brandon, A., Aitkenhead, N., Crofts, R.G., Ellison, R.A., Evans, D.J. & Riley, N. J. 1998. *Geology of the Country around Lancaster. Memoir for 1:50 000 geological sheet 59*. British Geological Survey. HMSO, London.

Catuneanu, O. 2002. Sequence stratigraphy of clastic systems: Concepts, merits, and pitfalls. *Journal of African Earth Sciences*, **35**, 1–43, https://doi.org/10.1016/S0899-5362(02)00004-0

Charpentier, B.R.R. & Cook, T.A. 2011. *USGS Methodology for Assessing Continuous Petroleum Resources.* U.S. Geological Survey Open-File Report 2011-1167.

Davies, S.J. 2008. The record of Carboniferous sea-level change in low-latitude sedimentary successions from Britain and Ireland during the onset of the late Paleozoic ice age. *In*: Fielding, C.R., Frank, T.D. & Isbell, J.L. (eds) *Resolving the Late Paleozoic Ice Age in Time and Space*. Geological Society of America, Special Papers, **441**, 187–204, https://doi.org/10.1130/2008.2441(13)

Davies, S.J., Leng, M.J., Macquaker, J.H.S. & Hawkins, K. 2012. Sedimentary process control on carbon isotope composition of sedimentary organic matter in an ancient shallow-water shelf succession. *Geochemistry, Geophysics, Geosystems*, **13**, 1–15, https://doi.org/10.1029/2012GC004218

Dembicki, H.J. 2009. Three common source rock evaluation errors made by geologists during prospect or play appraisals. *AAPG Bulletin*, **93**, 341–356, https://doi.org/10.1306/10230808076

Espitalié, J., Laporte, J.L., Madec, M., Marquis, F. & Leplat, P., Paulet, J. & Boutefeu, A. 1977. Méthode rapide de caractérisation des roches meres, de leur potentiel pétrolier et de leur degré d'évolution. *Revue de l'Institut Français du Pétrole*, **32**, 23–42.

Espitalié, J., Madec, M. & Tissot, B.P. 1980. Role of mineral matrix in kerogen pyrolysis: influence on petroleum generation and migration. *AAPG Bulletin*, **64**, 59–66.

Evans, D. & Kirby, G. 1999. The architecture of concealed Dinantian carbonate sequences over the Central Lancashire and Holme highs, northern England. *Proceedings of the Yorkshire Geological Society*, **52**, 297–312, https://doi.org/10.1144/pygs.52.3.297

Frank, T.D., Birgenheier, L.P., Montañez, I.P., Fielding, C.R. & Rygel, M.C. 2008. Late Paleozoic climate dynamics revealed by comparison of ice-proximal stratigraphic and ice-distal isotopic records. *In*: Fielding, C.R., Frank, T.D. & Isbell, J.L. (eds) *Resolving the Late Paleozoic Ice Age in Time and Space*. Geological Society of America, Special Papers, **441**, 1–12, https://doi.org/10.1130/2008.2441(23)

Fraser, A.J. & Gawthorpe, R.L. 1990. Tectono-stratigraphic development and hydrocarbon habitat of the Carboniferous in northern England. *In*: Hardman, R.F.P. & Brooks, J. (eds) *Tectonic Events Responsible for Britain's Oil and Gas Reserves*. Geological Society, London, Special Publications, **55**, 49–86.

Fraser, A.J. & Gawthorpe, R.L. 2003. *An Atlas of Carboniferous Basin Evolution in Northern England*. Geological Society, London, Memoirs, **28**.

Gabbott, S.E., Zalasiewicz, J., Aldridge, R.J. & Theron, J.N. 2010. Eolian input into the Late Ordovician postglacial Soom Shale, South Africa. *Geology*, **38**, 1103–1106, https://doi.org/10.1130/G31426.1

Gawthorpe, R.L. 1986. Sedimentation during carbonate ramp-to-slope evolution in a tectonically active area: Bowland Basin (Dinantian), northern England. *Sedimentology*, **33**, 185–206, https://doi.org/10.1111/j.1365-3091.1986.tb00531.x

Gawthorpe, R.L. 1987. Tectono-sedimentary evolution of the Bowland Basin, N England, during the Dinantian. *Journal of the Geological Society, London*, **144**, 59–71, https://doi.org/10.1144/gsjgs.144.1.0059

Gawthorpe, R., Hardy, S. & Ritchie, B. 2003. Numerical modelling of depositional sequences in half-graben rift basins. *Sedimentology*, **50**, 169–185.

Ghadeer, S.G. & Macquaker, J.H.S. 2012. The role of event beds in the preservation of organic carbon in fine-grained sediments: Analyses of the sedimentological processes operating during deposition of the Whitby Mudstone Formation (Toarcian, Lower Jurassic) preserved in northeast England. *Marine and Petroleum Geology*, **35**, 309–320, https://doi.org/10.1016/j.marpetgeo.2012.01.001

Gross, D., Sachsenhofer, R.F., Bechtel, A., Pytlak, L., Rupprecht, B. & Wegerer, E. 2015. Organic geochemistry of Mississippian shales (Bowland Shale Formation) in central Britain: Implications for depositional environment, source rock and gas shale potential. *Marine and Petroleum Geology*, **59**, 1–21, https://doi.org/10.1016/j.marpetgeo.2014.07.022

Hackley, P.C. & Cardott, B.J. 2016. Application of organic petrography in North American shale petroleum systems: A review. *International Journal of Coal Geology*, **163**, 8–51, https://doi.org/10.1016/j.coal.2016.06.010

Haq, B.U. & Schutter, S.R. 2008. A chronology of Paleozoic sea-level changes. *Science*, **322**, 64–69, https://doi.org/10.1126/science.1161648

Hart, B.S., Macquaker, J.H.S. & Taylor, K.G. 2013. Mudstone ('shale') depositional and diagenetic processes: Implications for seismic analyses of source-rock reservoirs. *Interpretation*, **1**, B7–B26, https://doi.org/10.1190/INT-2013-0003.1

Holdsworth, B.K. & Collinson, J.D. 1988. Millstone Grit cyclicity revisited. *In*: Besly, B.M. & Kelling, G. (eds) *Sedimentation in a Synorogenic Basin Complex: Upper Carboniferous of Northwest Europe*. Blackie, Glasgow, 132–152.

Howell, J.A. & Flint, S.S. 1996. A model for high resolution sequence stratigraphy within extensional basins. *In*: Howell, J. A. & Aitken, J.F. (eds) *High Resolution Sequence Stratigraphy: Innovations and Applications*. Geological Society, London, Special Publications, **104**, 129–137, https://doi.org/10.1144/GSL.SP.1996.104.01.09

Isbell, J.L., Miller, M.F., Wolfe, K.L. & Lenaker, P.A. 2003. Timing of late Paleozoic glaciation in Gondwana: Was glaciation responsible for the development of northern hemisphere cyclothems? *In*: Chan, M.A. & Archer, A.W. (eds) *Extreme Deposition Environments: Mega End Members in Geologic Time*. Geological Society of America, Special Papers, **370**, 5–24.

Jarvie, D.M. 2012. Shale resource systems for oil and gas: Part 1 – Shale-gas resource systems. *In*: Breyer, J.A. (ed.) *Shale Reservoirs – Giant Resources for the 21st Century*. AAPG Memoirs, **97**, 69–87, https://doi.org/10.1306/13321446M973489

Jarvie, D.M., Hill, R.J., Ruble, T.E. & Pollastro, R.M. 2007. Unconventional shale-gas systems: The Mississippian Barnett Shale of north–central Texas as one model for thermogenic shale-gas assessment. *AAPG Bulletin*, **91**, 475–499, https://doi.org/10.1306/12190606068

Kane, I.A. 2010. Development and flow structures of sand injectites: The Hind Sandstone Member injectite complex, Carboniferous, UK. *Marine and Petroleum Geology*, **27**, 1200–1215, https://doi.org/10.1016/j.marpetgeo.2010.02.009

Katz, B.J. 1983. Limitations of Rock-Eval pyrolysis for typing organic matter. *Organic Geochemistry*, **4**, 195–199.

Kirby, G.A., Baily, H.E. *et al.* 2000. *The Structure and Evolution of the Craven Basin and Adjacent Areas*. Subsurface Memoir of the British Geological Survey. HMSO, London.

Könitzer, S.F., Davies, S.J., Stephenson, M.H. & Leng, M.J. 2014. Depositional controls on mudstone lithofacies in a basinal setting: implications for the delivery of sedimentary organic matter. *Journal of Sedimentary Research*, **84**, 198–214, https://doi.org/10.2110/jsr.2014.18

Könitzer, S.F., Stephenson, M.H., Davies, S.J., Vane, C.H. & Leng, M.J. 2016. Significance of sedimentary organic matter input for shale gas generation potential of Mississippian Mudstones, Widmerpool Gulf, UK. *Review of Palaeobotany and Palynology*, **224**, 146–168, https://doi.org/10.1016/j.revpalbo.2015.10.003

Lazar, O.R., Bohacs, K.M., Macquaker, J.H.S., Schieber, J. & Demko, T.M. 2015*a*. Capturing key attributes of fine-grained sediment rocks in outcrops, cores, and thin sections: nomenclature and description guidelines. *Journal of Sedimentary Research*, **85**, 230–246, https://doi.org/10.2110/jsr.2015.11

Lazar, O.R., Bohacs, K., Schieber, J., Macquaker, J. & Demko, T. 2015*b*. Mudstone Primer: Lithofacies Variations, Diagnostic Criteria, and Sedimentologic-stratigraphic Implications at Lamina to Bedset Scales. *In: Concepts in sedimentology and paleontology*. SEPM Concepts in Sedimentology and Paleontology, **12**.

Loucks, R.G., Reed, R.M., Ruppel, S.C. & Jarvie, D.M. 2009. Morphology, genesis, and distribution of nanometer-scale pores in siliceous mudstones of the Mississippian Barnett Shale. *Journal of Sedimentary Research*, **79**, 848–861, https://doi.org/10.2110/jsr.2009.092

Loucks, R.G., Reed, R.M., Ruppel, S.C. & Hammes, U. 2012. Spectrum of pore types and networks in mudrocks and a descriptive classification for matrix-related mudrock pores. *AAPG Bulletin*, **96**, 1071–1098, https://doi.org/10.1306/08171111061

Macquaker, J.H.S., Taylor, K.G. & Gawthorpe, R.L. 2007. High-resolution facies analyses of mudstones: implications for paleoenvironmental and sequence stratigraphic interpretations of offshore ancient mud-dominated successions. *Journal of Sedimentary Research*, **77**, 324–339, https://doi.org/10.2110/jsr.2007.029

Macquaker, J.H.S., Bentley, S.J. & Bohacs, K.M. 2010. Wave-enhanced sediment-gravity flows and mud dispersal across continental shelves: Reappraising sediment transport processes operating in ancient mudstone successions. *Geology*, **38**, 947–950, https://doi.org/10.1130/G31093.1

McCave, I.N. & Jones, K.P. 1988. Deposition of ungraded muds from high-density non-turbulent turbidity currents. *Nature*, **333**, 250–252, https://doi.org/10.1038/333250a0

McIlreath, I.A. & James, N. 1978. Facies models 13. Carbonate slopes. *Geoscience Canada*, **5**.

Milliken, K. 2014. A compositional classification for grain assemblages in fine-grained sediments and sedimentary rocks. *Journal of Sedimentary Research*, **84**, 1185–1199.

Milliken, K.L., Esch, W.L., Reed, R.M. & Zhang, T. 2012. Grain assemblages and strong diagenetic overprinting in siliceous mudrocks, Barnett Shale (Mississippian), Fort Worth Basin, Texas. *AAPG Bulletin*, **96**, 1553–1578, https://doi.org/10.1306/12011111129

Mitchum, R.M.J. & Van Wagoner, J.C. 1991. High-frequency sequences and their stacking patterns: sequence stratigraphic evidence of high frequency eustatic cycles. *Sedimentary Geology*, **10**, 131–160.

Mitchum, R.M., Vail, P.R. & Thompson, S. 1977. Seismic stratigraphy and global changes of sea level, Part 2: The depositional sequence as a basic unit for

stratigraphic analysis. *In*: Payton, C.E. (ed.) *Seismic Stratigraphy – Applications to Hydrocarbon Exploration*. AAPG Memoirs, **26**, 53–62.
Newport, L.P., Aplin, A.C., Gluyas, J.G., Greenwell, H.C. & Grocke, D.R. 2016. Geochemical and lithological controls on a potential shale reservoir: Carboniferous Holywell Shale, Wales. *Marine and Petroleum Geology*, **71**, 198–210, https://doi.org/10.1016/j.marpetgeo.2015.11.026
Patruno, S., Hampson, G.J. & Jackson, C.A.L. 2015. Quantitative characterisation of deltaic and subaqueous clinoforms. *Earth-Science Reviews*, **142**, 79–119, https://doi.org/10.1016/j.earscirev.2015.01.004
Piper, D.W. 1978. Turbidite muds and silts on deep-sea fans and abyssal plains. *In*: Stanley, D.J. & Kelling, G. (eds) *Sedimentation in Submarine Canyons, Fans, and Trenches*. Hutchinson and Ross, Stroudsburg, Pennsylvannia, 163–176.
Ramsbottom, W.H.C. 1973. Transgressions and regressions in the Dinantian: a new synthesis of British Dinantian stratigraphy. *Proceedings of the Yorkshire Geological Society*, **39**, 567–607, https://doi.org/10.1144/pygs.39.4.567
Ramsbottom, W.H.C. 1978. Namurian mesothems in South Wales and northern France. *Journal of the Geological Society, London*, **135**, 307–312, https://doi.org/10.1144/gsjgs.135.3.0307
Ramsbottom, W.H.C. 1979. Rates of transgression and regression in the Carboniferous of NW Europe. *Journal of the Geological Society, London*, **136**, 147–153, https://doi.org/10.1144/gsjgs.136.2.0147
Ramsbottom, W.H.C. 1981. Eustacy, sea level and local tectonism, with examples from the British Carboniferous. *Proceedings of the Yorkshire Geological Society*, **43**, 473–482, https://doi.org/10.1144/pygs.43.4.473
Riley, N.J. 1988. *Stratigraphy of BP Minerals Borehole MHD11, Marl Hill, Whitewell, Lancs*. British Geological Survey Technical Report, WH/PD/88/304R.
Riley, N.J. 1990. Stratigraphy of the Worston Shale Group (Dinantian), Craven Basin, north-west England. *Proceedings of the Yorkshire Geological Society*, **48**, 163–187, https://doi.org/10.1144/pygs.48.2.163
Riley, N.J. 1993. Dinantian (Lower Carboniferous) biostratigraphy and chronostratigraphy in the British Isles. *Journal of the Geoloical Society, London*, **150**, 427–446, https://doi.org/10.1144/gsjgs.150.3.0427
Rohl, H.J., Schmid-Rohl, A., Oschmann, W., Frimmel, A. & Schwark, L. 2001. The Posidonia Shale (Lower Toarcian) of SW Germany: An oxygen depleted ecosystem ccontrolled by sea level and paleoclimate. *Palaeogeography, Palaeoclimatology, Palaeoecology*, **165**, 27–52.
Ross, D.J.K. & Bustin, R.M. 2009. The importance of shale composition and pore structure upon gas storage potential of shale gas reservoirs. *Marine and Petroleum Geology*, **26**, 916–927, https://doi.org/10.1016/j.marpetgeo.2008.06.004
Ross, C.A. & Ross, J.R.P. 1987. Late Paleozoic sea levels and depositional sequences. *Geology*, **61**, 137–149.
Rygel, M.C., Fielding, C.R., Frank, T.D. & Birgenheier, L.P. 2008. The magnitude of Late Paleozoic glacioeustatic fluctuations: a synthesis. *Journal of Sedimentary Research*, **78**, 500–511, https://doi.org/10.2110/jsr.2008.058
Schieber, J. 2007. Microbial mats on muddy substrates – examples of possible sedimentary features and underlying processes. *In*: Schieber, J., Bose, P.K., Eriksson, P.G., Banerjee, S., Sarkar, S., Altermann, W. & Catuneau, O. (eds) *Atlas of Microbial Mat Features Preserved within the Clastic Rock Record*. Elsevier, Amsterdam, 117–134.
Schieber, J. 2016*a*. Experimental testing of the transport-durability of shale lithics and its implications for interpreting the rock record. *Sedimentary Geology*, **331**, 162–169, https://doi.org/10.1016/j.sedgeo.2015.11.006
Schieber, J. 2016*b*. Mud re-distribution in epicontinental basins – Exploring likely processes. *Marine and Petroleum Geology*, **71**, 119–133, https://doi.org/10.1016/j.marpetgeo.2015.12.014
Schieber, J., Sur, S. & Banerjee, S. 2007. Benthic microbial mats in black shale units from the Vindhyan Supergroup, Middle Proterozoic of India: the challenges of recognizing the genuine article. *In*: Schieber, J., Bose, P.K., Eriksson, P.G., Banerjee, S., Sarkar, S., Altermann, W. & Catuneau, O. (eds) *An Atlas of Microbial Mat Features Preserved within the Clastic Rock Record*. Elsevier, Amsterdam, 189–197.
Schieber, J., Southard, J.B. & Schimmelmann, A. 2010. Lenticular shale fabrics resulting from intermittent erosion of water-rich muds – interpreting the rock record in the light of recent flume experiments. *Journal of Sedimentary Research*, **80**, 119–128, https://doi.org/10.2110/jsr.2010.005
Shanmugam, G. 2000. 50 years of the turbidite paradigm (1950s–1990s): deep water processes and facies models – a critical perspective. *Marine and Petroleum Geology*, **17**, 285–342, https://doi.org/10.1016/S0264-8172(99)00011-2
Somerville, I.D. 2008. Biostratigraphic zonation and correlation of Mississippian rocks in Western Europe: some case studies in the late Visean/Serpukhovian. *Geological Journal*, **43**, 209–240, https://doi.org/10.1002/gj.1097
Stephenson, M.H., Angliolini, L., Cozar, P., Jadoul, F., Leng, M.J., Millward, D. & Chenery, S. 2010. Northern England Serpukhovian (Early Namurian) farfield responses to southern hemisphere glaciation. *Journal of the Geological Society, London*, **167**, 1–14, https://doi.org/10.1144/0016-76492010-048
Stow, D.A.V. & Mayall, M. 2000. Deep-water sedimentary systems: New models for the 21st century. *Marine and Petroleum Geology*, **17**, 125–135.
Stow, D.A. & Piper, D.J. 1984. Deep-water fine-grained sediments: facies models. *In*: Stow, D.A.V. & Piper, D.J.W. (eds) *Fine-grained Sediments: Deep-water Processes and Facies*. Geological Society, London, Special Publications, **15**, 611–646, https://doi.org/10.1144/GSL.SP.1984.015.01.38
Stow, D.A.V & Shanmugam, G. 1980. Sequence of structures in fine-grained turbidites: comparison of recent deep-sea and ancient flysch sediments. *Sedimentary Geology*, **25**, 23–42.
Talling, P.J., Masson, D.G., Sumner, E.J. & Malgesini, G. 2012. Subaqueous sediment density flows: Depositional processes and deposit types. *Sedimentology*, **59**, 1937–2003, https://doi.org/10.1111/j.1365-3091.2012.01353.x
Taylor, K.G. & Macquaker, J.H.S. 2014. Diagenetic alterations in a silt- and clay-rich mudstone succession: an example from the Upper Cretaceous Mancos Shale of Utah, USA. *Clay Minerals*, **49**, 213–227, https://doi.org/10.1180/claymin.2014.049.2.05
Tissot, B.P. & Welte, D.H. 1984. *Petroleum Formation and Occurrence: A New Approach to Oil and Gas Exploration*, 2nd edn. Springer, Berlin.
Vail, P.R., Mitchum, R.M. & Thompson, S.I. 1977. Seismic stratigraphy and global changes of sea-level, Part 4: Global cycles of relative changes of sea level. *In*: Payton, C.E. (ed.) *Seismic Stratigraphy – Applications to Hydrocarbon Exploration*. AAPG Memoirs, **26**, 83–97.
Waters, C.N. & Condon, D.J. 2012. Nature and timing of Late Mississippian to Mid Pennsylvanian glacio-eustatic sea-level changes of the Pennine Basin, UK. *Journal of the Geological Society, London*, **169**, 37–51, https://doi.org/10.1144/jgs2013-055
Waters, C., Browne, M., Dean, M. & Powell, J. 2007. *Lithostratigraphical framework for Carboniferous successions of Great Britain (onshore)*. British Geological Survey, Nottingham, UK.
Waters, C.N., Waters, R.A., Barclay, W.J. & Davies, R.J. 2009. *A Lithostratigraphical Framework for the Carboniferous Successions of Southern Great Britain (Onshore)*. British Geological Survey, Nottingham, UK.
Waters, C.N., Somerville, I.D. *et al.* 2011. *A Revised Correlation of Carboniferous Rocks in the British Isles*. Geological Society, London, Special Reports, **26**.
Wignall, P.B. 1994. *Black Shales*. Oxford Monographs on Geology and Geophysics. Oxford University Press, Oxford.
Woodcock, N. & Strachan, R. (eds). 2002. *Geological History of Britain and Ireland*. Blackwell, Oxford.